Interactions between Boreal Summer Intraseasonal Oscillations and Synoptic-Scale Disturbances over the Western North Pacific. Part I: Energetics Diagnosis*

PANG-CHI HSU AND TIM LI

International Pacific Research Center, and School of Ocean and Earth Science and Technology, University of Hawaii at Manoa, Honolulu, Hawaii

CHIH-HUA TSOU

Department of Earth Science, National Taiwan Normal University, Taipei, Taiwan

(Manuscript received 7 May 2010, in final form 23 August 2010)

ABSTRACT

The role of scale interactions in the maintenance of eddy kinetic energy (EKE) during the extreme phases of the intraseasonal oscillation (ISO) is examined through the construction of a new eddy energetics diagnostic tool that separates the effects of ISO and a low-frequency background state (LFBS; with periods longer than 90 days). The LFBS always contributes positively toward the EKE in the boreal summer, regardless of the ISO phases. The synoptic eddies extract energy from the ISO during the ISO active phase. This positive barotropic energy conversion occurs when the synoptic eddies interact with low-level cyclonic and convergent–confluent ISO flows. This contrasts with the ISO suppressed phase during which the synoptic eddies lose kinetic energy to the ISO flow. The anticyclonic and divergent–diffluent ISO flows during the suppressed phase are responsible for the negative barotropic energy conversion.

A positive (negative) EKE tendency occurs during the ISO suppressed-to-active (active-to-suppressed) transitional phase. The cause of this asymmetric EKE tendency is attributed to the spatial phase relation among the ISO vorticity, eddy structure, and EKE. The southwest–northeast-tilted synoptic disturbances interacting with cyclonic (anticyclonic) vorticity of ISO lead to a positive (negative) EKE tendency in the northwest region of the maximum EKE center.

The genesis number and location and intensification rate of tropical cyclones in the western North Pacific are closely related to the barotropic energy conversion. The enhanced barotropic energy conversion favors the generation and development of synoptic seed disturbances, some of which eventually grow into tropical cyclones.

1. Introduction

The tropical troposphere exhibits a rich variety of temporal-scale variations, including interannual variability, the annual cycle, the intraseasonal oscillation (ISO), and the day-to-day fluctuation of synoptic-scale disturbances such as tropical cyclones (TCs) and tropical depression (TD)-type disturbances. These multiscale climate and weather systems have a large intensity during the boreal summer over the western North Pacific (WNP), and they may influence each other through complex scale interaction processes.

Many previous studies documented how the lower-frequency background flows modulate the synoptic-scale TC activity (e.g., Liebmann et al. 1994; Harr and Elsberry 1995; McBride 1995; Gray 1998; Ritchie and Holland 1999; Li et al. 2003; Li and Fu 2006; Fu et al. 2007). The summertime monsoon trough, with enhanced low-level cyclonic vorticity and wind confluence, plays an important role in the TC genesis and development over the WNP (McBride 1995; Gray 1998; Ritchie and Holland

* School of Ocean and Earth Science and Technology Contribution Number 8022 and International Pacific Research Center Contribution Number 722.

Corresponding author address: Tim Li, IPRC, SOEST, University of Hawaii at Manoa, 1680 East West Road, POST Bldg. 401, Honolulu, HI 96822.
E-mail: timli@hawaii.edu

DOI: 10.1175/2010JCLI3833.1

1999). The trajectories of TCs are primarily modulated by the large-scale environmental flow associated with both the monsoon trough and the subtropical high (Harr and Elsberry 1995). Besides the summer mean circulation, the ISO may significantly modulate the background flow pattern, creating a favorable or an unfavorable environment for the TC activity. For instance, Liebmann et al. (1994) found that the number of TCs increases (decreases) during the ISO active (suppressed) period. The genesis location and track of TCs are closely linked to the intraseasonal variation of large-scale circulation over the WNP (Kim et al. 2008; Chen et al. 2009).

The TD-type disturbances, often characterized as northwestward-propagating synoptic-scale wave trains, are frequently observed over the WNP (e.g., Lau and Lau 1990; Chang et al. 1996; Straub and Kiladis 2003; Li 2006; Tam and Li 2006). Embedded within the low-frequency ISO flow, the activity of the TD-type disturbances reveals a coherent intraseasonal variability. Straub and Kiladis (2003) indicated that the westward-propagating mixed Rossby–gravity (MRG)-TD-type wave activity is enhanced during the convectively active phase of the ISO. Maloney and Hartmann (2001) and Maloney and Dickinson (2003) found that the large-scale background flows modulated by the ISO substantially affect the energetics of TD-type disturbances. Enhanced low-level cyclonic shear and convergence favor the barotropic energy conversion from the mean flow to the synoptic-scale eddies.

While most previous studies focused on the large-scale controls of the mean circulation (Gray 1998) and/or the ISO flow (Liebmann et al. 1994; Maloney and Hartmann 2001) on the TC activity, there were few works addressing the upscale feedback of synoptic-scale motion and TCs to the mean flow or the low-frequency circulation. Straub and Kiladis (2003) found that the high-frequency disturbances and TCs may make up a significant portion of the ISO convective signal. By removing the TC vortices from the environmental flow in the National Centers for Environmental Prediction (NCEP) reanalysis data, Hsu et al. (2008) noted that ISO variance of 850-hPa vorticity is reduced to a great extent (more than 50%) along the TC tracks in the WNP. However, how TCs and synoptic-scale variability physically affect the ISO is not clear. Majda and Stechmann (2009) developed a simple theoretical model to demonstrate the nonlinear two-way interaction between large-scale intraseasonal flows and synoptic waves. The vertical tilted synoptic waves first transport momentum downscale and then upscale to large-scale flows, which regulates the sign of the intraseasonal zonal wind. Meanwhile, the propagating direction and strength of synoptic waves are controlled by the ISO flow.

The objective of this study is to document quantitatively to what extent and how the synoptic-scale disturbances feed back to the ISO. In Part I, we diagnose the upscale feedback from an energetics point of view, whereas in Hsu and Li (2011, hereafter Part II) we focus on the atmospheric apparent heat and moisture sources and the eddy momentum transport. Note that the eddy kinetic energy (EKE) budget equation used in Maloney and Hartmann (2001) and Maloney and Dickinson (2003) consists of only the interaction between the synoptic eddy and the mean flow. Here we develop a new approach to separate the background mean flow into a low-frequency background state (LFBS; with periods longer than 90 days) and an ISO component, so that one may diagnose the effects of the LFBS–eddy interaction and ISO–eddy interaction, respectively. The physical mechanisms responsible for the maintenance and development of EKE during the various phases of the ISO will be examined. The relationships between the energy conversion and the characteristics of synoptic disturbances including tropical cyclones are also examined.

The rest of this paper is organized as follows: section 2 describes the data and the analysis method. In section 3 a new eddy kinetic energy equation is derived, in an aim to separate the effects of the LFBS and ISO. The EKE diagnostic results with a focus on the ISO–synoptic eddy interaction are presented in section 4. The relationships between barotropic energy conversion and synoptic-scale seed disturbances associated with TC activity are shown in section 5. Finally, a summary is given in section 6.

2. Data and analysis methods

a. Data

The National Centers for Environmental Prediction–Department of Energy (DOE) reanalysis data (Kanamitsu et al. 2002) from 1979 to 2007 are adopted for the examinations of LFBS and ISO flows, and for the diagnoses of energy budget processes. Daily averaged zonal and meridional winds (u and v), pressure vertical velocity (ω), geopotential (ϕ), temperature (T), and pressure (p) at 17 pressure levels from 1000 to 100 hPa are utilized. The horizontal resolutions of these dynamic and thermodynamic variables are 2.5° longitude by 2.5° latitude.

The TC information is obtained from the Joint Typhoon Warning Center (JTWC; JTWC 2008). This dataset includes 6-hourly records of the longitude and latitude of TC location and its maximum wind speed. Only TCs with a maximum wind exceeding 17 m s^{-1} (tropical storm intensity) are considered for the calculation of the TC activity. Thus the term TC here comprises both the tropical storm and typhoon. To be comparable with the

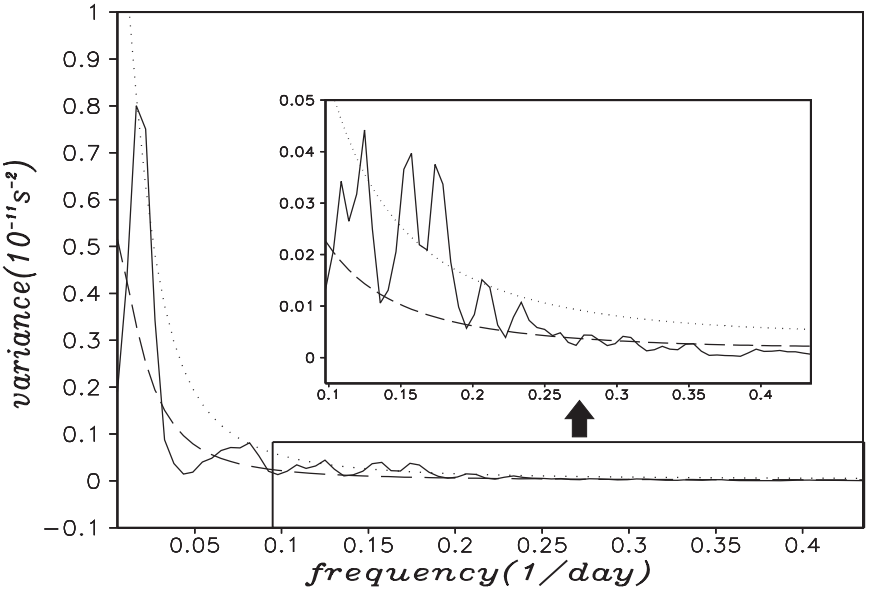

FIG. 1. Power spectrum of NCEP–DOE reanalysis 850-hPa vorticity during summer (July–September) for 1979–2007 over the WNP domain (0°–35°N, 110°–170°E). Long-dashed lines represent the red noise spectrum. Dotted line indicates 95% significance level. The annual cycle was removed before the computation of the spectrum.

daily reanalysis product, the TC information at 1200 UTC each day is used to calculate the TC activity.

b. Bandpass filtering and ISO phase definition

The fast Fourier transform (FFT) method is first utilized to illustrate the dominant spectrum peaks of the 850-hPa vorticity field over the WNP during the boreal summer. Because the variance of the annual cycle is much larger than other time-scale variabilities, it is removed prior to the spectrum calculation. The results of the vorticity spectrum show distinct peaks on the intraseasonal (10–90 day) and synoptic (<10 day) periods. Both the spectrum peaks are significant and above the red noise spectrum level and the 95% significance line (Fig. 1). Because of that, one may separate the original daily circulation fields into the LFBS, intraseasonal and synoptic-scale components.

To examine scale interactions among the LFBS, ISO, and synoptic-scale motion, the Butterworth bandpass filter (Hamming 1989) is used to extract the 10–90-day intraseasonal fluctuation, whereas a 10-day high-pass filter and a 90-day low-pass filter are applied to extract the synoptic disturbances and the LFBS signals from the raw data, respectively. To ensure that our decomposition method based on filtering guarantees the completeness (i.e., raw data = LFBS + ISO + synoptic motion), we compare the sum of the three filtered components with the raw data. As an example, we consider the time series of the vorticity averaged over the maximum variation region in the WNP from July to September in 1979–2007. The result shows that the time series of the sum of the three filtered components and raw data are almost identical (figure not shown). The difference between the two time series is very small, with a root-mean-square error of 1.5×10^{-10} m s^{-1}. Therefore, the filtering tools employed in this study are applicable to decomposition.

A singular value decomposition (SVD; Bretherton et al. 1992; Wallace et al. 1992) analysis is able to objectively identify a pair of patterns with a maximum temporal covariance. Here we apply this SVD analysis to the 10–90-day filtered 850-hPa vorticity and EKE fields for July–September during 1979–2007 over the WNP domain (0°–35°N, 110°–170°E). The first two SVD modes explain 77.5% of the covariance and are well separated from higher modes according to North et al. (1982). The temporal correlation between the vorticity and EKE time series of the leading SVD modes is quite high (0.7). A further analysis shows that the two leading SVD modes represent the different phases of the same physical mode, which is characterized by the northwestward propagation of a pair of vorticity and EKE fields over the WNP. A detailed description of the paired vorticity–EKE pattern is given in section 4. The analysis above points out a close linkage between the intraseasonal vorticity and EKE variances.

The active and suppressed phases of the ISO are stratified according to the SVD-1 time series of the 10–90-day filtered EKE field. The ISO active phase occurs when

the SVD-1 time series has a value greater than one standard deviation (1σ). A composite analysis shows that this phase is characterized by a strong EKE and a low-level cyclonic flow. The ISO suppressed phase is defined when the SVD-1 time series is less than -1 standard deviation. During this phase, a weak EKE and a low-level anticyclonic flow occur in the WNP. According to the definition above, 358 and 317 days are selected for the ISO active and suppressed phase composites, respectively, during July–September of 1979–2007.

A suppressed-to-active (active-to-suppressed) transitional phase is further defined when the SVD-1 time series lies in between -0.25 and 0.25σ and is between two well-defined active and suppressed peaks, both of which exceed one standard deviation. The so-defined composite cases for the suppressed-to-active and active-to-suppressed transitional phases are 39 and 43 days, respectively.

c. Measuring TC activity

The TC activity is measured based on the TC genesis number and location and the growth−decay rate. The TC genesis is defined when the JTWC named TC is first reported. The TC growth–decay rate is defined as the difference of the maximum wind speed at a 1-day interval. A positive (negative) value indicates the growth (decay) of the TC intensity. A composite is made for ISO active and suppressed phases to illustrate the dependence of the TC activity on the ISO.

3. A new EKE diagnostic tool for examining the eddy–ISO interaction

In this section an eddy kinetic energy budget equation is derived to investigate the dynamic processes responsible for the maintenance and development of the synoptic-scale eddies during the various phases of the ISO. Different from the previous studies (e.g., Maloney and Hartmann 2001), we separate the effects of the eddy interactions with the LFBS and the ISO. A dependent variable may be separated into three components, the LFBS (90 day or longer), intraseasonal (10–90 day), and synoptic-scale (below 10 day) parts:

$$A = \overline{\overline{A}} + \tilde{A} + A', \tag{1}$$

where a double overbar denotes the LFBS field, a tilde overbar denotes the intraseasonal component, and a prime denotes the synoptic-scale field.

By multiplying u' and v' in both sides of the synoptic-scale momentum equations, one may derive the perturbation EKE equation, which consists of multiscale interactions among the LFBS, ISO, and synoptic-scale motion:

$$\begin{aligned}\frac{\partial K'}{\partial t} = &-u'\left(\frac{\partial \overline{\overline{u}}}{\partial t} + \frac{\partial \tilde{u}}{\partial t}\right) - v'\left(\frac{\partial \overline{\overline{v}}}{\partial t} + \frac{\partial \tilde{v}}{\partial t}\right) - u'(\overline{\overline{u}} + \tilde{u} + u')\left(\frac{\partial \overline{\overline{u}}}{\partial x} + \frac{\partial \tilde{u}}{\partial x} + \frac{\partial u'}{\partial x}\right) - v'(\overline{\overline{u}} + \tilde{u} + u')\left(\frac{\partial \overline{\overline{v}}}{\partial x} + \frac{\partial \tilde{v}}{\partial x} + \frac{\partial v'}{\partial x}\right)\\ &- u'(\overline{\overline{v}} + \tilde{v} + v')\left(\frac{\partial \overline{\overline{u}}}{\partial y} + \frac{\partial \tilde{u}}{\partial y} + \frac{\partial u'}{\partial y}\right) - v'(\overline{\overline{v}} + \tilde{v} + v')\left(\frac{\partial \overline{\overline{v}}}{\partial y} + \frac{\partial \tilde{v}}{\partial y} + \frac{\partial v'}{\partial y}\right) - u'(\overline{\overline{\omega}} + \tilde{\omega} + \omega')\left(\frac{\partial \overline{\overline{u}}}{\partial p} + \frac{\partial \tilde{u}}{\partial p} + \frac{\partial u'}{\partial p}\right)\\ &- v'(\overline{\overline{\omega}} + \tilde{\omega} + \omega')\left(\frac{\partial \overline{\overline{v}}}{\partial p} + \frac{\partial \tilde{v}}{\partial p} + \frac{\partial v'}{\partial p}\right) - u'\left(\frac{\partial \overline{\overline{\phi}}}{\partial x} + \frac{\partial \tilde{\phi}}{\partial x} + \frac{\partial \phi'}{\partial x}\right) - v'\left(\frac{\partial \overline{\overline{\phi}}}{\partial y} + \frac{\partial \tilde{\phi}}{\partial y} + \frac{\partial \phi'}{\partial y}\right),\end{aligned} \tag{2}$$

where $K' = (u'^2 + v'^2)/2$ is the synoptic EKE, t is time, u is zonal wind, v is meridional wind, ω is vertical velocity, p is pressure, and ϕ is geopotential. The dissipation and subgrid-scale processes are not considered in this study.

Apply a 10-day low-pass filtering operator (denoted by a single overbar) to the perturbation EKE equation above. The following terms can be dropped:

$$-\overline{u'\left(\frac{\partial \overline{\overline{u}}}{\partial t} + \frac{\partial \tilde{u}}{\partial t}\right)} = -\overline{u'\frac{\partial \overline{\overline{u}}}{\partial t}} = 0,$$

$$-\overline{v'\left(\frac{\partial \overline{\overline{v}}}{\partial t} + \frac{\partial \tilde{v}}{\partial t}\right)} = -\overline{v'\frac{\partial \overline{\overline{v}}}{\partial t}} = 0,$$

$$-\overline{u'\left(\frac{\partial \overline{\overline{\phi}}}{\partial x} + \frac{\partial \tilde{\phi}}{\partial x}\right)} = -\overline{u'\frac{\partial \overline{\overline{\phi}}}{\partial x}} = 0, \quad \text{and}$$

$$-\overline{v'\left(\frac{\partial \overline{\overline{\phi}}}{\partial y} + \frac{\partial \tilde{\phi}}{\partial y}\right)} = -\overline{v'\frac{\partial \overline{\overline{\phi}}}{\partial y}} = 0.$$

Then a low-frequency EKE budget equation may be derived as follows:

$$\frac{\partial \overline{K'}}{\partial t} = \mathrm{CK} + \mathrm{CA} + \mathrm{AM} + \mathrm{AE} + \mathrm{FG} \tag{3}$$

$$\mathrm{CK} = -\overline{\mathbf{V}' \cdot [(\overline{\overline{\mathbf{V}}}_3 + \tilde{\mathbf{V}}_3 + \mathbf{V}'_3) \cdot \nabla_3]\overline{\overline{\mathbf{V}}}} - \overline{\mathbf{V}' \cdot [(\overline{\overline{\mathbf{V}}}_3 + \tilde{\mathbf{V}}_3 + \mathbf{V}'_3) \cdot \nabla_3]\tilde{\mathbf{V}}}$$

$$= -\left(\begin{array}{l} \overline{u'\overline{\overline{u}}\frac{\partial \overline{\overline{u}}}{\partial x}} + \overline{v'\overline{\overline{u}}\frac{\partial \overline{\overline{v}}}{\partial x}} + \overline{u'\overline{\overline{v}}\frac{\partial \overline{\overline{u}}}{\partial y}} + \overline{v'\overline{\overline{v}}\frac{\partial \overline{\overline{v}}}{\partial y}} + \overline{u'\overline{\overline{\omega}}\frac{\partial \overline{\overline{u}}}{\partial p}} + \overline{v'\overline{\overline{\omega}}\frac{\partial \overline{\overline{v}}}{\partial p}} + \overline{u'\tilde{u}\frac{\partial \overline{\overline{u}}}{\partial x}} + \overline{v'\tilde{u}\frac{\partial \overline{\overline{v}}}{\partial x}} + \overline{u'\tilde{v}\frac{\partial \overline{\overline{u}}}{\partial y}} + \overline{v'\tilde{v}\frac{\partial \overline{\overline{v}}}{\partial y}} + \overline{u'\tilde{\omega}\frac{\partial \overline{\overline{u}}}{\partial p}} \\ + \overline{v'\tilde{\omega}\frac{\partial \overline{\overline{v}}}{\partial p}} + \overline{u'^2\frac{\partial \overline{\overline{u}}}{\partial x}} + \overline{v'u'\frac{\partial \overline{\overline{v}}}{\partial x}} + \overline{u'v'\frac{\partial \overline{\overline{u}}}{\partial y}} + \overline{v'^2\frac{\partial \overline{\overline{v}}}{\partial y}} + \overline{u'\omega'\frac{\partial \overline{\overline{u}}}{\partial p}} + \overline{v'\omega'\frac{\partial \overline{\overline{v}}}{\partial p}} + \overline{u'\overline{\overline{u}}\frac{\partial \tilde{u}}{\partial x}} + \overline{v'\overline{\overline{u}}\frac{\partial \tilde{v}}{\partial x}} + \overline{u'\overline{\overline{v}}\frac{\partial \tilde{u}}{\partial y}} \\ + \overline{v'\overline{\overline{v}}\frac{\partial \tilde{v}}{\partial y}} + \overline{u'\overline{\overline{\omega}}\frac{\partial \tilde{u}}{\partial p}} + \overline{v'\overline{\overline{\omega}}\frac{\partial \tilde{v}}{\partial p}} + \overline{u'\tilde{u}\frac{\partial \tilde{u}}{\partial x}} + \overline{v'\tilde{u}\frac{\partial \tilde{v}}{\partial x}} + \overline{u'\tilde{v}\frac{\partial \tilde{u}}{\partial y}} + \overline{v'\tilde{v}\frac{\partial \tilde{v}}{\partial y}} + \overline{u'\tilde{\omega}\frac{\partial \tilde{u}}{\partial p}} + \overline{v'\tilde{\omega}\frac{\partial \tilde{v}}{\partial p}} + \overline{u'^2\frac{\partial \tilde{u}}{\partial x}} \\ + \overline{v'u'\frac{\partial \tilde{v}}{\partial x}} + \overline{u'v'\frac{\partial \tilde{u}}{\partial y}} + \overline{v'^2\frac{\partial \tilde{v}}{\partial y}} + \overline{u'\omega'\frac{\partial \tilde{u}}{\partial p}} + \overline{v'\omega'\frac{\partial \tilde{v}}{\partial p}} \end{array} \right)$$

$$\mathrm{CA} = -\frac{R}{p}\overline{T'\omega'},$$

$$\mathrm{AM} = \mathrm{AMm} + \mathrm{AMi} = -\overline{\overline{\mathbf{V}}_3 \cdot \nabla_3 K'} - \overline{\tilde{\mathbf{V}}_3 \cdot \nabla_3 K'},$$

$$\mathrm{AE} = -\overline{\mathbf{V}'_3 \cdot \nabla_3 K'}, \quad \text{and}$$

$$\mathrm{FG} = -\overline{\nabla_3 \cdot (\mathbf{V}'_3 \phi')}$$

where a single overbar represents the 10-day low-pass filtering operator, $\overline{K'}$ is the low-frequency EKE (including both the LFBS and ISO components), $\mathbf{V}$ is the horizontal velocity vector, ∇ is the horizontal gradient operator (the subscript 3 represents the three-dimensional components), R is the gas constant for dry air, and T is temperature.

Equation (3) shows that various processes may affect the tendency of the low-frequency EKE ($\overline{K'}$). The physical meaning of each term at the right-hand side of Eq. (3) is described as follows: the term CK represents the barotropic energy conversion from the LFBS and ISO flows to the high-frequency synoptic-scale eddy. CA indicates the baroclinic energy conversion from eddy available potential energy (EAPE) to EKE as an air parcel ascends (descends) in a warmer (colder) region. The quantity AM represents the advections of EKE by both the LFBS (AMm) and the ISO (AMi) flows. AE represents the advection of EKE by the synoptic-scale eddy. FG denotes the generation of EKE through the convergence of eddy geopotential fluxes.

In the equation above, only the CK and AM terms depend on the product of the background flow and eddy fields, and thus these two terms explicitly reflect the eddy–mean flow interactions. However, the other terms reflect the eddy–eddy interactions and thus become effective in changing the EKE only after eddies have been significantly modulated by the mean flow change. A further comparison of CK and AM indicates that CK is the major generation term for the low-frequency EKE, while AM mainly redistributes the EKE through the mean flow advection. It is worth mentioning that the diabatic heating is a major EAPE source for synoptic-scale disturbances, which is ultimately transformed to EKE (Lau and Lau 1992). This process is implicitly reflected in the FG term. The physical argument is that even without the CK and AM contributions, the ISO circulation makes synoptic-scale heating more or less likely depending on its phase, which can further affect the strength of the synoptic eddies and thus EKE. However, because of the lack of a clear mathematical formula for the diabatic heating, it is difficult to quantitatively measure its effect. A strategy will be developed in Part II of this study to investigate this heating effect by diagnosing the apparent heat and moisture sources and sinks.

The left-hand side of Eq. (3) consists of the sum of the EKE tendencies on both the LFBS and ISO time scales. Applying a 90-day low-pass filter onto Eq. (3) and assuming $\overline{\partial \tilde{K}'/\partial t} = 0$, one may derive an LFBS EKE tendency equation as below:

$$\frac{\partial \overline{\overline{K'}}}{\partial t} = \overline{\overline{\mathrm{CK}}} + \overline{\overline{\mathrm{CA}}} + \overline{\overline{\mathrm{AM}}} + \overline{\overline{\mathrm{AE}}} + \overline{\overline{\mathrm{FG}}}. \tag{4}$$

Subtracting the LFBS EKE tendency from Eq. (3), one may derive the time change rate of EKE on the intraseasonal time scale, that is,

$$\frac{\partial \tilde{K}'}{\partial t} = \Delta\mathrm{CK} + \Delta\mathrm{CA} + \Delta\mathrm{AM} + \Delta\mathrm{AE} + \Delta\mathrm{FG}, \tag{5}$$

where $\Delta()$ denotes the difference between () and $\overline{\overline{()}}$. Equation (5) directly measures how the eddy kinetic energy changes on the intraseasonal time scale. By calculating the difference terms at the right-hand side of Eq. (5) for each of the ISO phases, one may examine how the EKE is maintained and what the major energy conversion processes are that contribute to the EKE tendency.

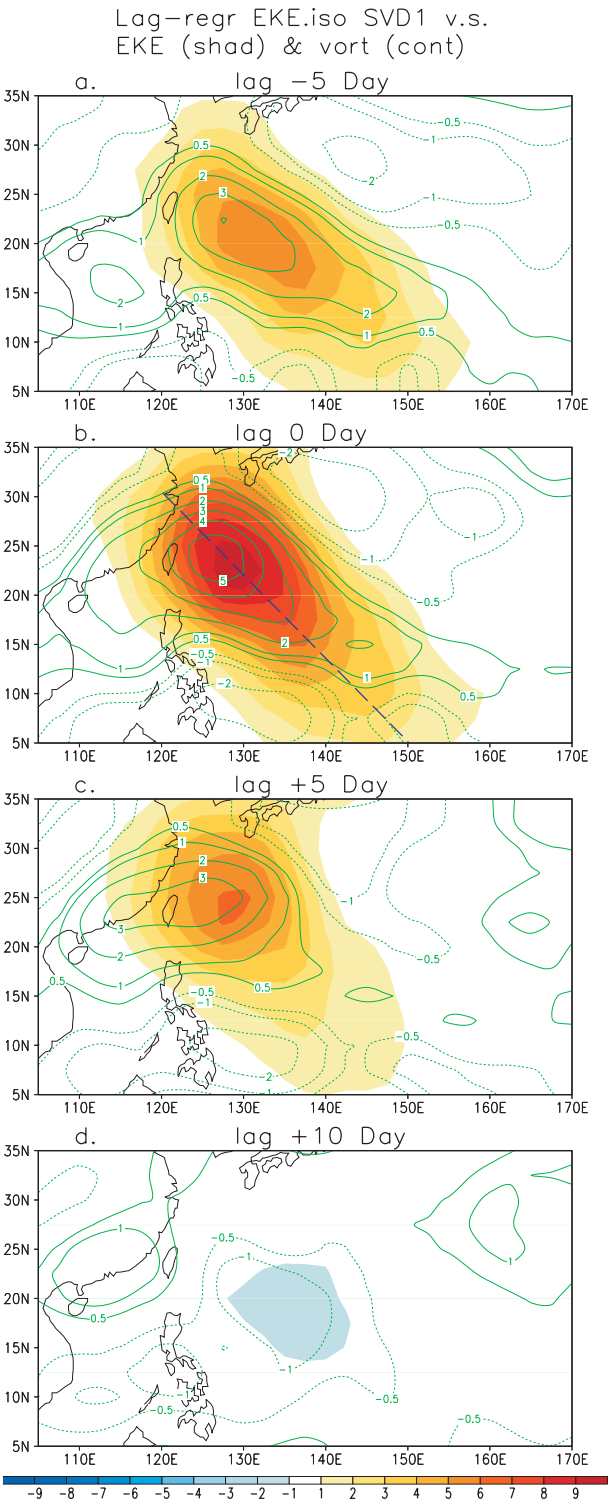

FIG. 2. Regressed 10–90-day filtered 850-hPa EKE (shading; $m^2\ s^{-2}$) and vorticity (contour; $10^{-6}\ s^{-1}$) fields at a lag of (a) −5, (b) 0, (c) +5, and (d) +10 days. The regression is based on the SVD-1 time series of the filtered 850-hPa EKE field.

4. Maintenance and development of EKE during various ISO phases

a. Evolution patterns of the intraseasonal EKE variability

To reveal the temporal and spatial phase relationships between the ISO vorticity and EKE, we calculate the lagged regression patterns of the 10–90-day filtered vorticity and EKE fields with the SVD-1 EKE time series from July to September for 1979–2007 (Fig. 2). The lagged regression result indicates that both the ISO vorticity and EKE centers move northwestward in the WNP. Such a northwestward propagation is consistent with previous observational studies (e.g., Wang and Rui 1990; Kemball-Cook and Wang 2001; Hsu and Weng 2001). It is interesting to note that the maximum cyclonic vorticity center is located to the northwest of the maximum EKE center. This implies that for a fixed location, the ISO vorticity leads the EKE. Both the intraseasonal vorticity and EKE fields have their maximum amplitudes at day 0, indicating a simultaneous strengthening between them. The result above is consistent with Maloney and Hartmann (2001), who found that the EKE is enhanced (decreased) in the ISO westerly (easterly) phase.

As the EKE has a maximum (minimum) value during the ISO active (suppressed) phase, the EKE tendency is positive (negative) during the ISO transition phase from a suppressed (active) to an active (suppressed) phase. This points out an asymmetric EKE tendency between the two ISO transitional phases. In the following, we will examine the specific processes that maintain the EKE during the ISO extreme phases, and the mechanisms that lead to the asymmetric EKE tendency during the transitional phases.

b. Maintenance of EKE during the ISO extreme phases

Figure 3 shows the vertical structure of the intraseasonal EKE during the ISO active and suppressed phases along the southeastward axis of the largest EKE variance shown in Fig. 2b. Two maximum EKE centers are found during the ISO active phase, with one being in the upper troposphere around 150 hPa and the other being in the lower troposphere near 850 hPa (Fig. 3a). During the ISO suppressed phase, the EKE is weakened throughout the troposphere (Fig. 3b). In both the phases, the maximum changes of EKE occur in the lower troposphere. Because of that, in the following we will focus on the diagnosis of the low-level EKE budget, with special attention on energy conversion processes that maintain the EKE amplitude during the ISO active and suppressed phases.

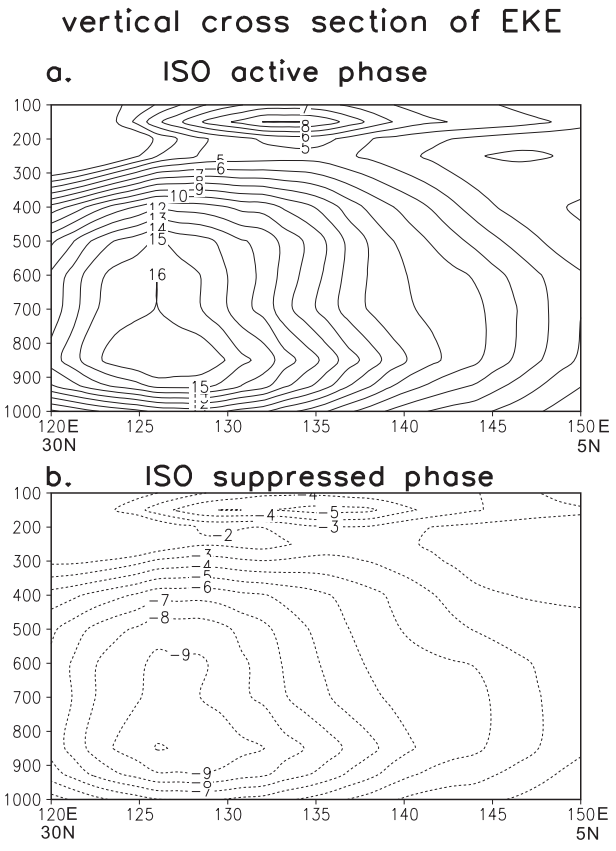

FIG. 3. Vertical cross sections of the intraseasonal EKE during the ISO (a) active and (b) suppressed phases along the axis (dashed line) shown in Fig. 2b (m^2 s^{-2}).

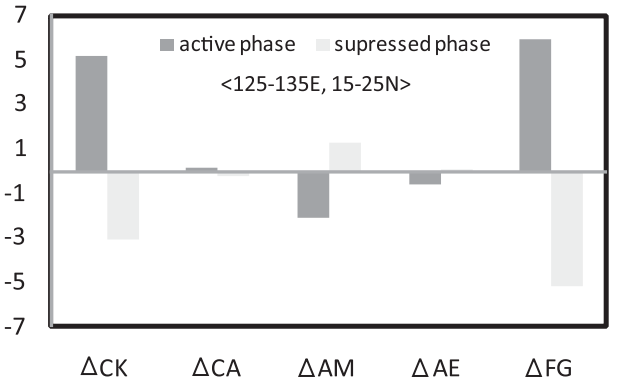

FIG. 4. Intraseasonal EKE budget terms at 850 hPa averaged over a box (15°–25°N, 125°–135°E) during the ISO active (dark gray bars) and suppressed (light gray bars) phases (10^{-5} m^2 s^{-3}).

Figure 4 presents the relative contributions of 850-hPa EKE tendency terms at the right-hand side of Eq. (5), averaged over the maximum intraseasonal EKE variation region (15°–25°N, 125°–135°E). It is found that both the barotropic energy conversion (ΔCK) and ΔFG associated with the convergence of eddy geopotential fluxes are major terms that contribute to a positive EKE tendency during the ISO active phase. While its major effect on the energy source is in the upper troposphere (Lau and Lau 1992; Hsu et al. 2009), ΔCA shows a small positive contribution in the low-level EKE budget. Thus ΔCA is meaningful and can be related to ΔFG when one integrates this term over the depth of the troposphere (Lau and Lau 1992). The EKE advections through the large-scale background circulation (ΔAM) and synoptic-scale eddy (ΔAE) contribute to a negative EKE tendency. The budget terms during the ISO active and suppressed phases approximately exhibit an out-of-phase relationship. The negative ΔCK and ΔFG terms account for the decrease of EKE during the ISO suppressed phase.

As the term ΔCK affects the intraseasonal EKE tendency through direct eddy–mean flow interactions, we will focus on the diagnosis of this barotropic energy conversion term. A key question related to the eddy–mean flow interaction is what the relative contribution of the barotropic energy conversion by the LFBS ($\overline{\overline{CK}}$) and ISO (ΔCK) flows is. Figure 5 illustrates the active and suppressed phase composites and their difference in the low-frequency barotropic energy conversion (CK) and the relative contributions of $\overline{\overline{CK}}$ and ΔCK. Note that CK is positive during both the ISO active and suppressed phases (Figs. 5a,b), indicating that the combined LFBS and ISO flow always contributes positively to the EKE. The difference of CK between the ISO active and suppressed phase (Fig. 5c) approximately removes the LFBS effect; it shows an enhanced barotropic energy conversion from ISO to eddy during the ISO active phase. Such a difference cannot identify the asymmetry of energy conversion between the active and suppressed ISO phase. With the methodology applied in deriving Eqs. (4) and (5), one may readily illustrate the relative contributions of the barotropic energy conversions by the LFBS (Fig. 5d) and ISO flows and the asymmetry between the active and suppressed ISO phase (Figs. 5e,f). The result shows that $\overline{\overline{CK}}$ has large positive values over the WNP during the boreal summer (Fig. 5d). This indicates that the barotropic energy conversion due to the LFBS–ISO–eddy interaction on the LFBS time scale always contributes positively to the EKE growth. In other words, the LFBS keeps providing kinetic energy for synoptic eddy development over the tropical WNP, regardless of the ISO active or suppressed phases. In contrast, the ΔCK term, which mainly describes the barotropic energy conversion in association with the ISO variation, indicates a phase-dependent feature. Figures 5e and 5f reveal an out-of-phase barotropic energy conversion between the two extreme ISO phases. This indicates that while the synoptic disturbances extract kinetic energy from the ISO during the ISO active phase (Fig. 5e),

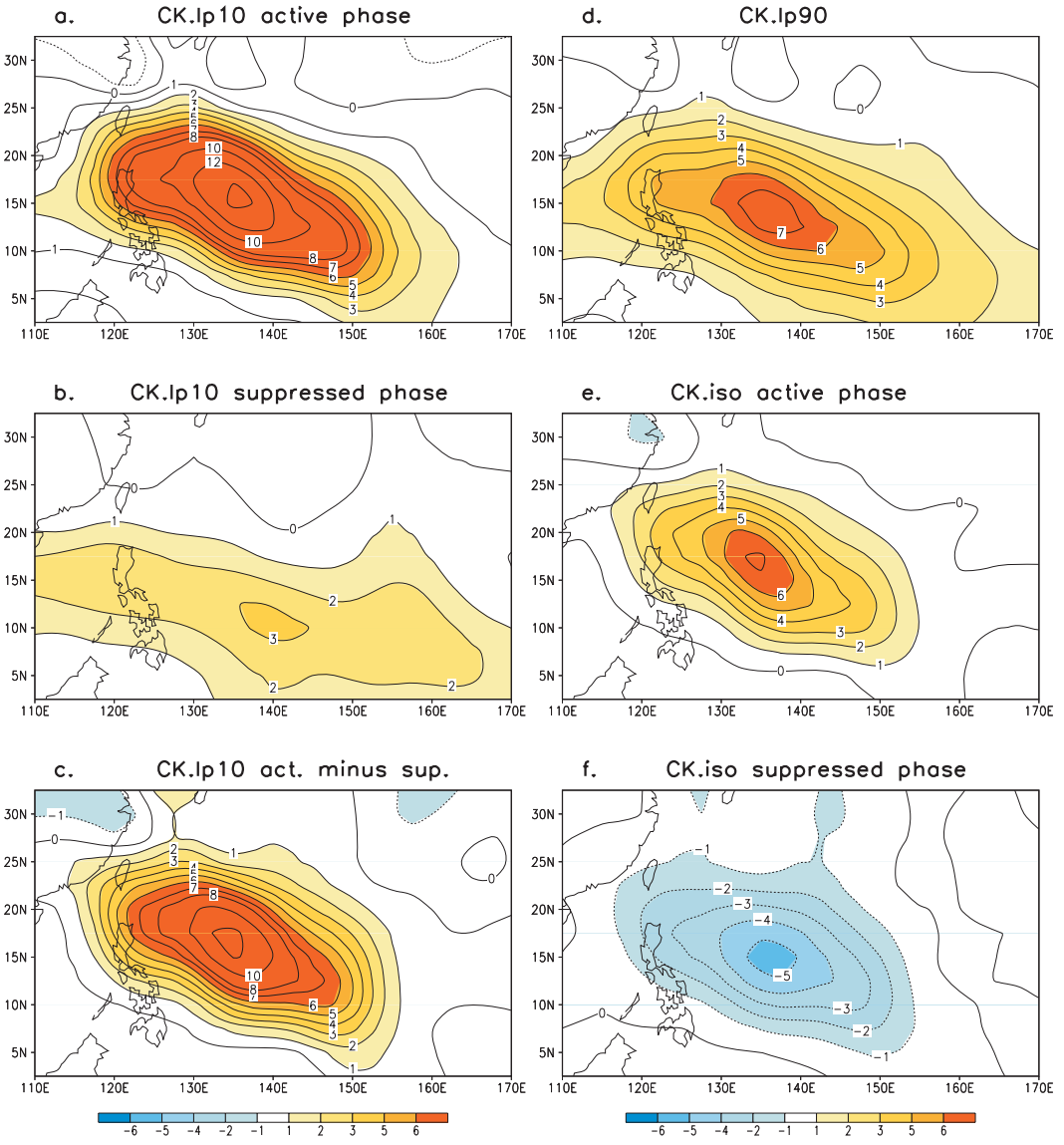

FIG. 5. Composite CK at 850 hPa during the ISO (a) active and (b) suppressed phases and (c) their difference. (d) The 850-hPa $\overline{CK}$ averaged during July–September, (e) 850-hPa ΔCK during the ISO active phase, and (f) 850-hPa ΔCK during the ISO suppressed phase (10^{-5} m^2 s^{-3}).

they lose energy to the ISO during the ISO suppressed phase (Fig. 5f). This might be part of the reason why EKE is greater (smaller) during the ISO active (suppressed) phase. Thus, the above analysis reveals from the energetics point of view that there exists a two-way interaction between the ISO and synoptic-scale disturbances over the WNP; that is, synoptic-scale motions may gain (provide) energy from (to) the ISO, depending on the phases of the ISO.

To understand the specific process that gives rise to the phase-dependent energy conversion, we further examine each barotropic conversion term separately. Among 36 terms of barotropic energy conversion [see CK in Eq. (3)], four terms associated with the interaction between horizontal eddy momentum fluxes and ISO flows are dominant terms, which account for 80% of the total ΔCK over the maximum EKE variance center. Figure 6 depicts the four dominant ΔCK terms $\{\Delta[-\overline{u'^2(\partial\tilde{u}/\partial x)}]$, $\Delta[-\overline{v'^2(\partial\tilde{v}/\partial y)}]$, $\Delta[-\overline{u'v'(\partial\tilde{u}/\partial y)}]$, and $\Delta[-\overline{u'v'(\partial\tilde{v}/\partial x)}]\}$, and the associated ISO circulations for the ISO active phase composite. Since the dominant synoptic-scale variability in the WNP is characterized by a northeast–southwest-tilted wave train, we have $u'v' > 0$. Given that $u'v' > 0$, $u'^2 > 0$, and $v'^2 > 0$, the sign of term

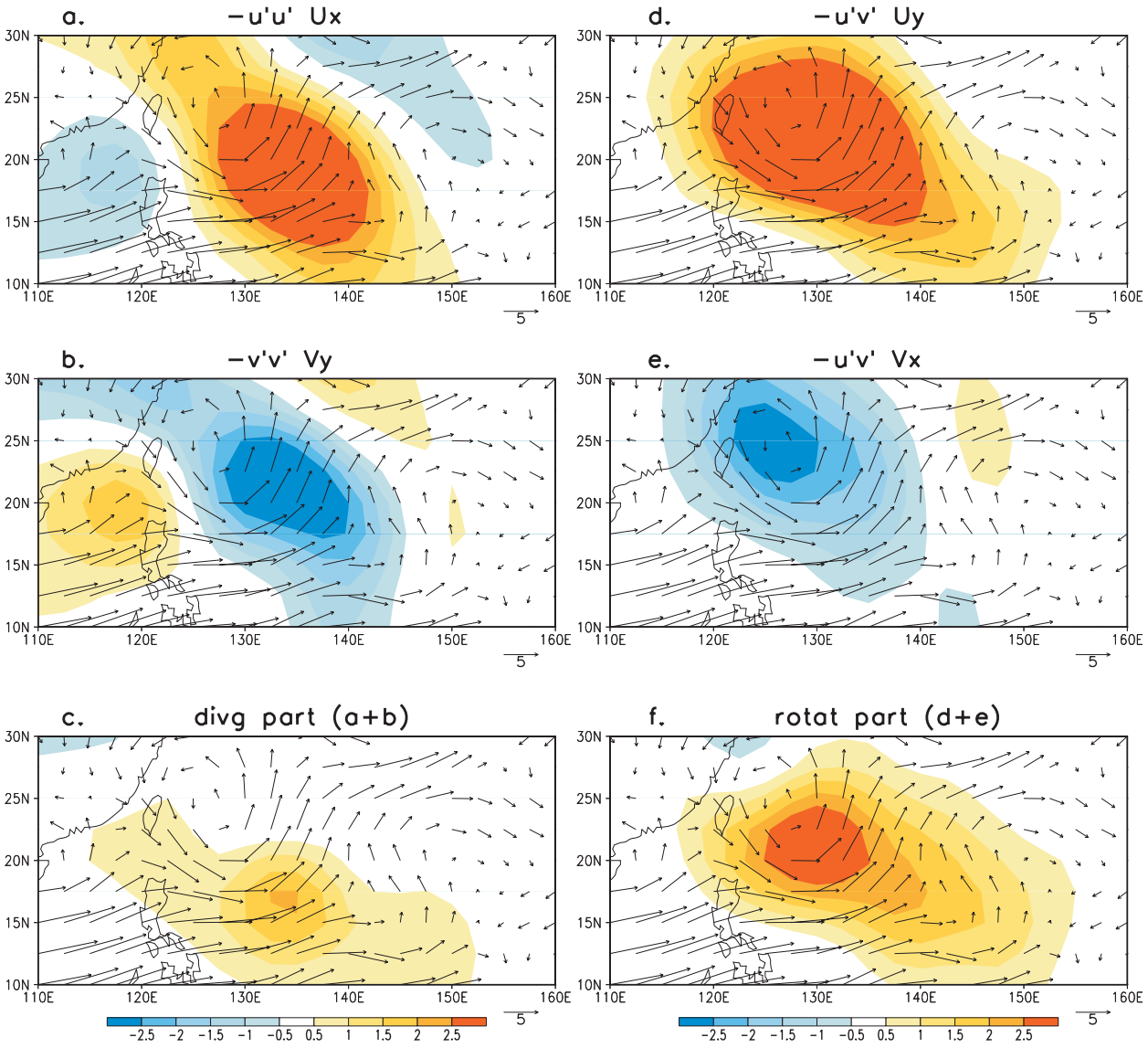

FIG. 6. Individual components (a) $\Delta[-\overline{u'^2(\partial\tilde{u}/\partial x)}]$, (b) $\Delta[-\overline{v'^2(\partial\tilde{v}/\partial y)}]$, (d) $\Delta[-\overline{u'v'(\partial\tilde{u}/\partial y)}]$, and (e) $\Delta[-\overline{u'v'(\partial\tilde{v}/\partial x)}]$ of 850-hPa ΔCK (shading; 10^{-5} m^2 s^{-3}) and 850-hPa ISO wind (vector; m s^{-1}) during the ISO active phase. Sum of 850-hPa ΔCK induced by ISO (c) divergent–diffluent and (f) rotational flows.

ΔCK is determined by the gradients of the ISO flow. The positive ΔCK induced by $\Delta[-\overline{u'^2(\partial\tilde{u}/\partial x)}]$ is mainly located in the downstream regions of the strong ISO westerly, where the zonal gradient of the ISO westerly is negative (Fig. 6a). The ISO zonal wind convergence favors the growth of high-frequency transient eddies through barotropic wave accumulation, as discussed in previous studies (e.g., Sobel and Bretherton 1999; Kuo et al. 2001; Tam and Li 2006). In a similar way, the convergence–confluence of the ISO meridional flow over the South China Sea leads to a positive ΔCK through $\Delta[-\overline{v'^2(\partial\tilde{v}/\partial y)}]$ (Fig. 6b). The combination of both the ISO convergence–confluence terms causes a positive barotropic energy conversion in the WNP (Fig. 6c). In addition, the rotational components of the ISO flow may also contribute to the enhanced ΔCK during the ISO active phase. Our calculation shows that a large positive ΔCK appears in the ISO cyclonic shear region ($\partial\tilde{u}/\partial y < 0$) over the WNP (Fig. 6d). Although the barotropic energy conversion associated with the zonal gradient of the ISO meridional flow $\Delta[-\overline{u'v'(\partial\tilde{v}/\partial x)}]$ is negative (Fig. 6e), its magnitude is smaller and the net contribution from the rotational parts of the ISO flow is positive (Fig. 6f). The overall comparison of Figs. 6c and 6f indicates that the net effect of the ISO rotational flow is greater in contributing to the EKE tendency than that due to the

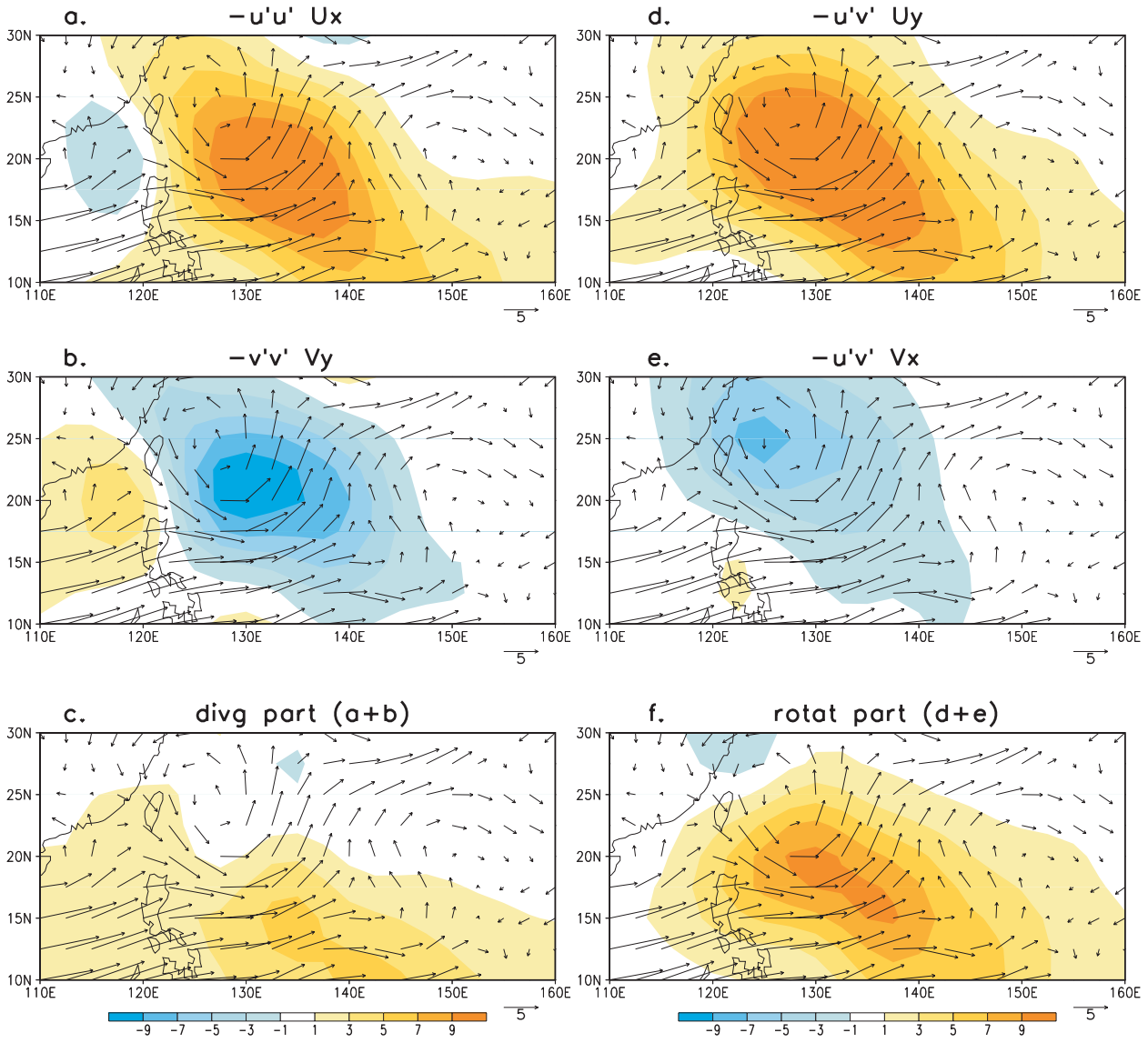

FIG. 7. As in Fig. 6, but for CK.

ISO convergent–confluent flow. Similar but opposite-sign patterns are found during the ISO suppressed phase when the divergent–diffluent and anticyclonic low-level flows appear over the WNP (figure not shown).

To compare with each of the ΔCK terms above, we also plot the corresponding CK terms during the ISO active phase in Fig. 7. The result shows that they generally have a similar pattern, but with a larger amplitude. This suggests that the ISO flow and the LFBS flow act in a similar way to strengthen the barotropic energy conversion. The individual CK terms during the ISO suppressed phase (figure not shown) are weaker than those during the ISO active phase, because the ISO flow during its suppressed phase tends to reduce the LFBS flow effect.

In summary, the synoptic-scale eddies gain kinetic energy from both the LFBS and the ISO during the ISO active phase, while they extract kinetic energy from the LFBS but give up the energy to the ISO during the ISO suppressed phase. This two-way energy conversion is primarily ascribed to the alternation of the ISO cyclonic–confluent and anticyclonic–diffluent flows interacting with the northeast–southwest-tilted synoptic wave train over the WNP.

c. *Cause of asymmetric EKE tendencies between the ISO transitional phases*

A positive (negative) EKE tendency occurs during the ISO suppressed-to-active (active-to-suppressed) transition phase. What causes the asymmetry? Addressing the

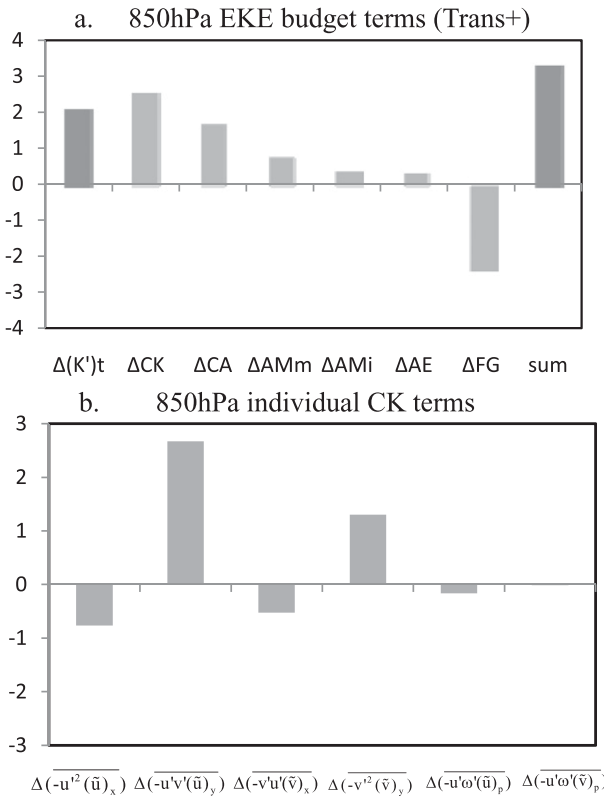

FIG. 8. (a) Individual 850-hPa intraseasonal EKE tendency (10^{-5} m^2 s^{-3}) terms averaged at 15°–25°N and 125°–135°E for the suppressed-to-active transitional phase composite; the leftmost shows the observed tendency, whereas the rightmost shows the sum of all budget terms. (b) As in (a), but for the individual components of ΔCK.

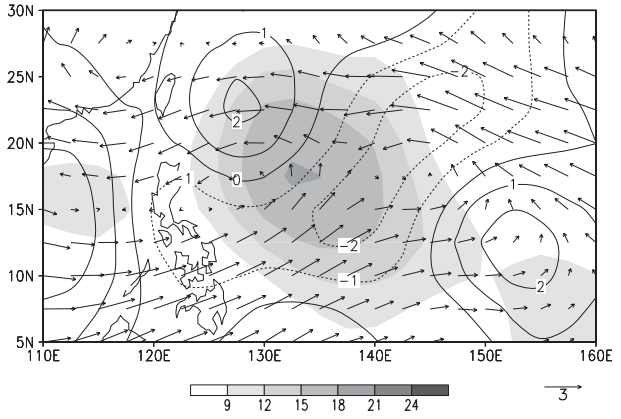

FIG. 9. The composite ISO wind (vector; m s^{-1}), 3–10-day vorticity (contour; 10^{-6} s^{-1}), and EKE (shading; m^2 s^{-2}) fields at 850 hPa during the ISO suppressed-to-active transitional phase.

question is essential to understand why EKE retains the maximum value during the ISO active phase. To reveal the dynamic mechanisms that cause the asymmetric EKE tendency, we examine the EKE budget terms during the ISO suppressed-to-active and active-to-suppressed transitional phases over the maximum EKE variance region (15°–25°N, 125°–135°E). Figure 8 shows the EKE budget terms during the suppressed-to-active transition. Note that all terms except the eddy geopotential flux term account for the positive EKE tendency. The sum of these terms, although somewhat overestimated, is consistent with the observed EKE tendency.

A further analysis of the barotropic conversion terms indicates that the positive EKE tendency results mainly from the meridional gradient of the ISO zonal and meridional flows (Fig. 8b). To understand how the eddy–ISO interaction contributes to the EKE growth, we illustrate the relationship between southwest–northeast-tilted synoptic-scale waves and intraseasonal circulations during that transitional phase. As shown in Fig. 9, the positive eddy momentum fluxes (u'^2, v'^2 and $u'v'$) interacting with the cyclonic flows of the ISO generate a positive barotropic energy conversion in the northwest region of the EKE center. This spatial phase relation between the synoptic eddy and the ISO flow provides a dynamic explanation as to how the barotropic conversion processes during the ISO transitional phase contribute to the positive EKE tendency. A similar budget but with an opposite sign and a weaker amplitude is found during the active-to-suppressed transitional phase.

5. Relationship between the barotropic energy conversion and tropical cyclone activity

The EKE diagnosis in section 4 indicates that while the LFBS always provides energy for eddies to grow, the ISO flow loses (gains) energy to (from) eddies during the ISO active (suppressed) phase. Does this phase-dependent energy conversion process affect synoptic seed disturbances and associated TC activity? In this section, we examine how TC genesis location and number and growth–decay rate are modulated by the ISO from an energetics perspective.

The distributions of the total barotropic energy conversion ($CK = \overline{\overline{CK}} + \Delta CK$) and the genesis location of TCs during different ISO phases are presented in Fig. 10. The positive CK appears for both the ISO active and suppressed phases, indicating that the embedded synoptic-scale disturbances always obtain kinetic energy from the total background flows. Regions of enhanced CK favor the development of synoptic seed disturbances, which may further grow into TCs. Figure 10 illustrates that WNP TCs tend to form in the positive CK regions during both the active and suppressed phases. The amplitude and spatial pattern of CK vary with the ISO phases. Because of the positive contribution of CK from both the LFBS

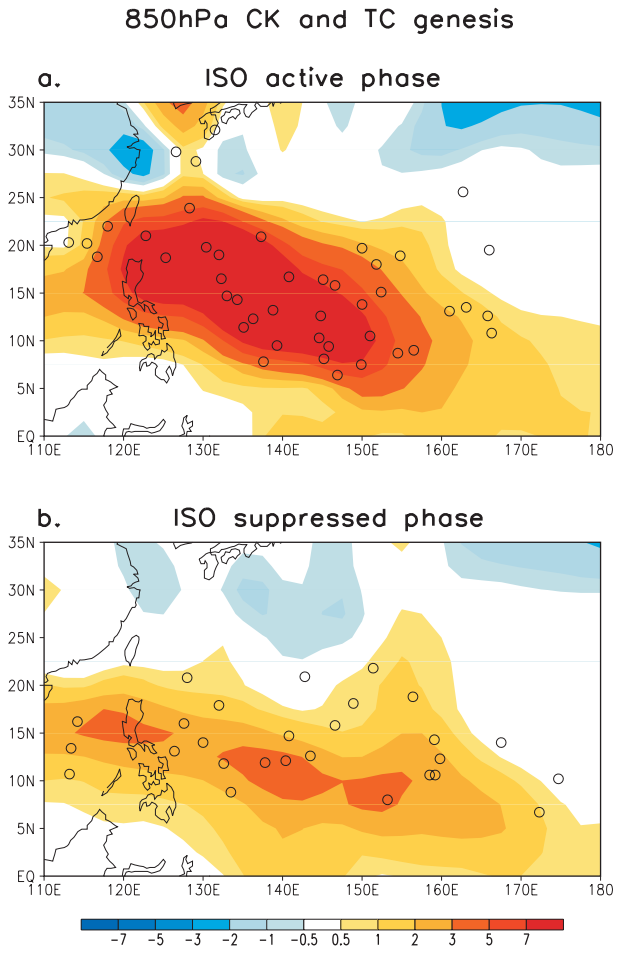

FIG. 10. Composites of 850-hPa CK (shading; 10^{-5} m^2 s^{-3}) and TC genesis location (circle) for the ISO (a) active and (b) suppressed phases.

and ISO flows during the ISO active phase, a larger CK occurs over the WNP south of 25°N (Fig. 10a). During the ISO suppressed phase, the negative ΔCK offsets the large part of the positive $\overline{CK}$ (Fig. 5). As a result a smaller positive CK appears over the WNP (Fig. 10b).

The TC genesis number and location are closely related to the EKE tendency associated with the barotropic energy conversion. For example, the number of TC geneses during the ISO active phase is 43, which is about 1.5 times greater than that during the ISO suppressed phase (27). This result is in accord with the ratio of 850-hPa CK averaged over the WNP region (10°–20°N, 120°–160°E). More TCs formed north of 20°N—as the maximum CK center shifts northward—during the ISO active phase than during the ISO suppressed phase (Fig. 10).

Figure 11 further reveals the relationship between the barotropic energy conversion and TC intensification rate. In general, more (less) rapidly intensified TCs are observed during the ISO active (suppressed) phase, when CK is greater (smaller). Figure 12 is a scatter diagram illustrating how the TC developing rate depends on the CK. There is a positive correlation between them. The correlation coefficients are 0.35 and 0.34 for the ISO active and suppressed phases, respectively, both of which are significant at the 99% level. The result indicates that more TCs with larger growth rates (>30 kt day^{-1}) occur during the ISO active phase (Fig. 12a) than during the ISO suppressed phase (Fig. 12b). It is worth mentioning that unlike Hsu et al. (2008), in the mean flow calculation we did not remove TC vortices from the reanalysis fields. While both Figs. 11 and 12 show the observed relationship, caution is needed to interpret the result, as the intensity change of a mature TC is mainly attributed to latent heating. It is not clear whether the background flow directly affects TC strength through the barotropic energy conversion or if it is the change of background conditions (such as moisture and boundary layer convergence) associated with ISO that affects the TC intensity change.

6. Summary

Both the ISO and the synoptic-scale disturbances are vigorous over the WNP in the boreal summer. A lagged regression analysis indicates that both the ISO vorticity and the EKE propagate northwestward in the WNP and that the cyclonic vorticity center is located to the northwest of the maximum EKE center. The maximum EKE difference between the ISO active and suppressed phases appears in the lower troposphere (near 850 hPa).

A new EKE diagnosis tool is developed in which we separate the background mean flow into the LFBS and ISO components. By subtracting the 90-day low-pass filtered EKE budget terms [Eq. (4)] from the original low-frequency EKE tendency equation [Eq. (3)], one may remove the LFBS contribution and focus on the eddy–ISO interaction. Our diagnosis reveals that the increased (decreased) EKE arises from the barotropic energy conversion and the convergence of eddy geopotential fluxes during the ISO active (suppressed) phase. The eddy geopotential flux term is primarily related to diabatic heating, which will be discussed in Part II. In this paper, we focus on the barotropic energy conversion and associated eddy–mean flow interactions.

The barotropic energy conversions on the LFBS and intraseasonal time scales are diagnosed separately. The results reveal that mean flow–eddy interaction on the LFBS time scale contributes positively toward the EKE growth in the boreal summer regardless of the ISO phases. This implies that the summer mean flows always favor the growth of synoptic-scale disturbances over the WNP through the barotropic energy conversion. The

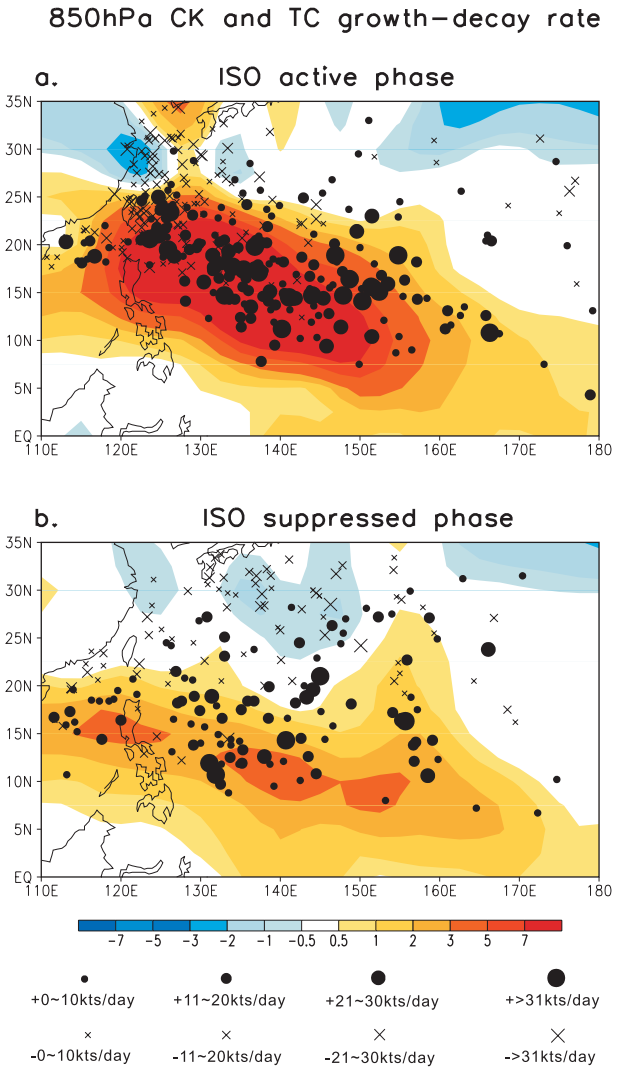

FIG. 11. As in Fig. 10, except that the dot and multiplication signs indicate the TC growth and decay rates (unit: knots day^{-1}), respectively. The size of the signs is proportional to the growth–decay rate.

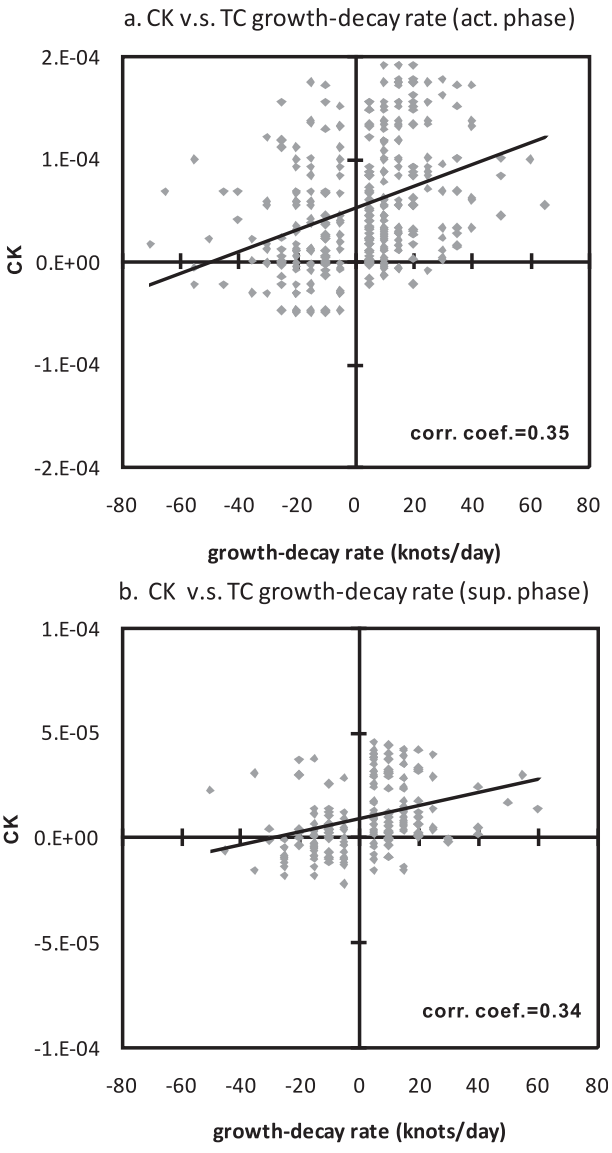

FIG. 12. A scatter diagram of the TC growth–decay rate (knots day^{-1}) vs the local 850-hPa CK (m^2 s^{-3}) during the ISO (a) active and (b) suppressed phases. The linear trends and correlation coefficients are shown.

CK on the intraseasonal time scale, however, reveals a two-way energy conversion between the ISO and synoptic-scale eddies, depending on the ISO phases. The high-frequency eddy may gain kinetic energy from the ISO during its active phase, while it gives up its energy to the ISO during its suppressed phase. The barotropic energy conversion associated with the eddy–ISO interaction depends on both the eddy and ISO structures. Because the low-level synoptic-scale eddy exhibits a northeast–southwest-tilted structure (e.g., Lau and Lau 1990), the signs of eddy momentum fluxes are always positive. Thus the ISO circulation patterns may greatly influence the barotropic energy conversion. The convergent ($\partial\tilde{u}/\partial x < 0$) and cyclonic ($\partial\tilde{u}/\partial y < 0$) low-level flows during the ISO active phase may create a favorable environment for the growth of synoptic-scale disturbances. In contrast, a divergent–diffluent and anticyclonic flow during the ISO suppressed phase may suppress the eddy development and lead to energy loss of the ISO.

The EKE diagnostics shows a positive (negative) EKE tendency during the ISO transition from a suppressed (active) to an active (suppressed) phase. The cause of this asymmetry is attributed to the difference in the barotropic energy conversion associated with the ISO–eddy interaction. The southwest–northeast-tilted synoptic disturbances interacting with the cyclonic flow of ISO lead

to a positive EKE tendency in the northwest region of the EKE center. An opposite pattern appears during the active-to-suppressed phase transition.

The barotropic energy conversion associated with the eddy–mean flow interaction is closely related to the TC activity in the WNP. The increased (decreased) barotropic energy conversion during the ISO active (suppressed) phase is consistent with a larger (smaller) TC genesis number; the TC genesis number during the ISO active phase is about 1.5 times greater than that during the ISO suppressed phase. More TCs with a growth rate exceeding 30 kt day^{-1} occur during the ISO active phase. The results support the notion that the TD-type disturbances that gain energy from the mean flow may provide the seed disturbances for cyclogenesis during the ISO active phase (Maloney and Hartmann 2001).

In this part, we focus on the synoptic eddy–ISO interaction from an energetics point of view. The role of diabatic heating will be further investigated in Part II of this study, based on the diagnoses of the atmospheric apparent heat and moisture sources. In addition to the aforementioned processes, the synoptic-scale motion may exert an upscale feedback to the ISO through the eddy momentum transport, the nonlinear rectification of the surface latent heat flux (Zhou and Li 2010), and/or the change of the SST (e.g., Lin et al. 2003; Li et al. 2008). The relative importance of these processes will be investigated in future studies.

Acknowledgments. The authors thank the two anonymous reviewers for constructive comments that led to a much improved manuscript. This work was supported by NSC97-2917-I-564-154, NSC-097-2811-M-003-015, ONR Grants N000140810256 and N000141010774, and by the International Pacific Research Center that is sponsored by the Japan Agency for Marine-Earth Science and Technology (JAMSTEC), NASA (NNX07AG53G), and NOAA (NA17RJ1230).

REFERENCES

Bretherton, C. S., C. Smith, and J. M. Wallace, 1992: An intercomparison of methods for finding coupled patterns in climate data. *J. Climate,* **5,** 541–560.

Chang, C.-P., J. M. Chen, P. A. Harr, and L. E. Carr, 1996: Northwestward-propagating wave patterns over the tropical western North Pacific during summer. *Mon. Wea. Rev.,* **124,** 2245–2266.

Chen, T. C., S. Y. Wang, M. C. Yen, and A. J. Clark, 2009: Impact of the intraseasonal variability of the western North Pacific large-scale circulation on tropical cyclone tracks. *Wea. Forecasting,* **24,** 646–666.

Fu, B., T. Li, M. Peng, and F. Weng, 2007: Analysis of tropical cyclone genesis in the western North Pacific for 2000 and 2001. *Wea. Forecasting,* **22,** 763–780.

Gray, W. M., 1998: The formation of tropical cyclones. *Meteor. Atmos. Phys.,* **67,** 37–69.

Hamming, R. W., 1989: *Digital Filters*. Prentice-Hall, 284 pp.

Harr, P. A., and R. L. Elsberry, 1995: Large-scale circulation variability over the tropical western North Pacific. Part I: Spatial patterns and tropical cyclone characteristics. *Mon. Wea. Rev.,* **123,** 1225–1246.

Hsu, H.-H., and C.-H. Weng, 2001: Northwestward propagation of the intraseasonal oscillation in the western North Pacific during the boreal summer: Structure and mechanism. *J. Climate,* **14,** 3834–3850.

——, C. H. Hung, A. K. Lo, C. C. Wu, and C. W. Hung, 2008: Influence of tropical cyclones on the estimation of climate variability in the tropical western North Pacific. *J. Climate,* **21,** 2960–2975.

Hsu, P.-C., and T. Li, 2011: Interactions between boreal summer intraseasonal oscillations and synoptic-scale disturbances over the western North Pacific. Part II: Apparent heat and moisture sources and eddy momentum transport. *J. Climate,* **24,** 940–959.

——, C.-H. Tsou, H.-H. Hsu, and J.-H. Chen, 2009: Eddy energy along the tropical storm track in association with ENSO. *J. Meteor. Soc. Japan,* **87,** 687–704.

JTWC, cited 2008: Joint Typhoon Warning Center best track data site. [Available online at http://www.usno.navy.mil/NOOC/nmfc-ph/RSS/jtwc/best_tracks/.]

Kanamitsu, M., W. Ebisuzaki, J. Woollen, S.-K. Yang, J. J. Hnilo, M. Fiorino, and G. L. Potter, 2002: NCEP-DOE AMIP-II reanalysis (R-2). *Bull. Amer. Meteor. Soc.,* **83,** 1631–1643.

Kemball-Cook, S., and B. Wang, 2001: Equatorial waves and air–sea interaction in the boreal summer intraseasonal oscillation. *J. Climate,* **14,** 2923–2942.

Kim, J. H., C. H. Ho, H. S. Kim, C. H. Sui, and S. K. Park, 2008: Systematic variation of summertime tropical cyclone activity in the western North Pacific in relation to the Madden–Julian oscillation. *J. Climate,* **21,** 1171–1191.

Kuo, H. C., J. H. Chen, R. T. Williams, and C. P. Chang, 2001: Rossby waves in zonally opposing mean flow: Behavior in northwest Pacific summer monsoon. *J. Atmos. Sci.,* **58,** 1035–1050.

Lau, K.-H., and N.-C. Lau, 1990: Observed structure and propagation characteristics of tropical summertime synoptic-scale disturbances. *Mon. Wea. Rev.,* **118,** 1888–1913.

——, and ——, 1992: The energetics and propagation dynamics of tropical summertime synoptic-scale disturbances. *Mon. Wea. Rev.,* **120,** 2523–2539.

Li, T., 2006: Origin of the summertime synoptic-scale wave train in the western North Pacific. *J. Atmos. Sci.,* **63,** 1093–1102.

——, and B. Fu, 2006: Tropical cyclogenesis associated with Rossby wave energy dispersion of a preexisting typhoon. Part I: Satellite data analyses. *J. Atmos. Sci.,* **63,** 1377–1389.

——, ——, X. Ge, B. Wang, and M. Peng, 2003: Satellite data analysis and numerical simulation of tropical cyclone formation. *Geophys. Res. Lett.,* **30,** 2122, doi:10.1029/2003GL018556.

——, F. Tam, X. Fu, T. Zhou, and W. Zhu, 2008: Causes of the intraseasonal SST variability in the tropical Indian Ocean. *Atmos.–Ocean Sci. Lett.,* **1,** 18–23.

Liebmann, B., H. H. Hendon, and J. D. Glick, 1994: The relationship between tropical cyclones of the western Pacific and Indian Oceans and the Madden-Julian oscillation. *J. Meteor. Soc. Japan,* **72,** 401–411.

Lin, I.-I., W. T. Liu, C.-C. Wu, J. C. H. Chiang, and C.-H. Sui, 2003: Satellite observations of modulation of surface winds by typhoon-induced upper ocean cooling. *Geophys. Res. Lett.,* **30,** 1131, doi:10.1029/2002GL015674.

Majda, A. J., and S. N. Stechmann, 2009: A simple dynamical model with features of convective momentum transport. *J. Atmos. Sci.,* **66,** 373–392.

Maloney, E. D., and D. L. Hartmann, 2001: The Madden–Julian oscillation, barotropic dynamics, and North Pacific tropical cyclone formation. Part I: Observations. *J. Atmos. Sci.,* **58,** 2545–2558.

——, and M. J. Dickinson, 2003: The intraseasonal oscillation and the energetics of summertime tropical western North Pacific synoptic-scale disturbances. *J. Atmos. Sci.,* **60,** 2153–2168.

McBride, J. L., 1995: Tropical cyclone formation. Global Perspective on Tropical Cyclones, R. L. Elsberry, Ed., WMO Tech. Doc. 693, World Meteorological Organization, 63–105.

North, G. R., T. L. Bell, R. F. Cahalan, and F. J. Moeng, 1982: Sampling errors in the estimation of empirical orthogonal functions. *Mon. Wea. Rev.,* **110,** 699–706.

Ritchie, E. A., and G. J. Holland, 1999: Large-scale patterns associated with tropical cyclogenesis in the western Pacific. *Mon. Wea. Rev.,* **127,** 2027–2043.

Sobel, A. H., and C. S. Bretherton, 1999: Development of synoptic-scale disturbances over the summertime tropical northwest Pacific. *J. Atmos. Sci.,* **56,** 3106–3127.

Straub, K. H., and G. N. Kiladis, 2003: Interactions between the boreal summer intraseasonal oscillation and higher-frequency tropical wave activity. *Mon. Wea. Rev.,* **131,** 945–960.

Tam, C.-Y., and T. Li, 2006: The origin and dispersion characteristics of the observed summertime synoptic-scale waves over the western Pacific. *Mon. Wea. Rev.,* **134,** 1630–1646.

Wallace, J. M., C. Smith, and C. S. Bretherton, 1992: Singular value decomposition of wintertime sea surface temperature and 500-mb height anomalies. *J. Climate,* **5,** 561–576.

Wang, B., and H. Rui, 1990: Synoptic climatology of transient tropical intraseasonal convection anomalies: 1975-1985. *Meteor. Atmos. Phys.,* **44,** 43–61.

Zhou, C., and T. Li, 2010: Upscale feedback of tropical synoptic variability to intraseasonal oscillations through the nonlinear rectification of the surface latent heat flux. *J. Climate,* **23,** 5738–5754.